# Supplementary Information: Last Glacial Maximum World-Ocean simulations at eddy-permitting and coarse resolutions: Do eddies contribute to a better consistency between models and paleo-proxies ?

M. Ballarotta[1], L. Brodeau[1], J. Brandefelt[2], P. Lundberg[1], and K. Döös[1]

[1]Department of Meteorology/Oceanography, Stockholm University, 106 91 Stockholm, Sweden

[2]Department of Mechanics, KTH (Royal Institute of Technology), 106 91 Stockholm, Sweden

*Correspondence to:* M. Ballarotta (maxime.ballarotta@natgeo.su.se)

This supplementary part includes the Figures S1 to S16 and Table S1.

Figure S1 supplements Figures 1 and 2 by showing the regions where the permitted eddies have an impact on the LGM sea-ice state. The mid-latitude regions (North Atlantic, North Pacific and ACC) are the main regions sensitive to the eddy regime.
Figure S2 supplements Figure 5 by showing the regions of different sea-ice thickness between the eddy-permitting and the coarse resolution experiments. In the Northern hemisphere the difference in sea-ice mainly results in the difference of volume (sea-ice thickness larger in the eddy-permitting experiment). In the southern hemisphere it is mainly the difference in the fraction of sea-ice along the ACC.
Figure S3 supplements Figure 6 by representing the boreal winter and boreal summer deep mixed layers in the coarse resolution simulation.
Figure S4 supplements Figure 7 by showing the zonally averaged temperature in the Atlantic basin as well as the corresponding AMOC for the coarse and eddy-permitting simulations.
Figures S5 to S13 supplement Figures 9 to 12. They represent the Taylor diagrams for coarse and eddy-permitting hindcast simulations of the 1958-2006 period. Note that these hindcast simulations have been performed with the NEMO model (ORCA1 and ORCA025) forced with the Drakkar Forcing Set 4.3 (Brodeau et al., 2010). The World Ocean Atlas 1998 dataset is then used for the statistical tests. On one hand, Figures S5 to S9 show that the eddy-permitting hindcast simulation improves the statistical scores for representing the observed SSTs, particularly in the 25°N-50°N band and the annually averaged tropical SSTs. On the other hand, Figures S10 to S13 reveal that the improvements diagnosed when using the global SST dataset are less obvious when considering only the modern SSTs at the MARGO core locations.
Figures S14 to S16 supplement Table 2. They represent the scatter plots of the simulated ORCA1 and ORCA025 SSTs versus reconstructed SST and corresponding statistical values in the Agulhas, the Gulf Stream and Kuroshio regions.
Finally, the linear regression tests (for the modern SSTs) applied in specific regions (western boundary currents and Antarctic Circumpolar Current) are summarized in Table S1.

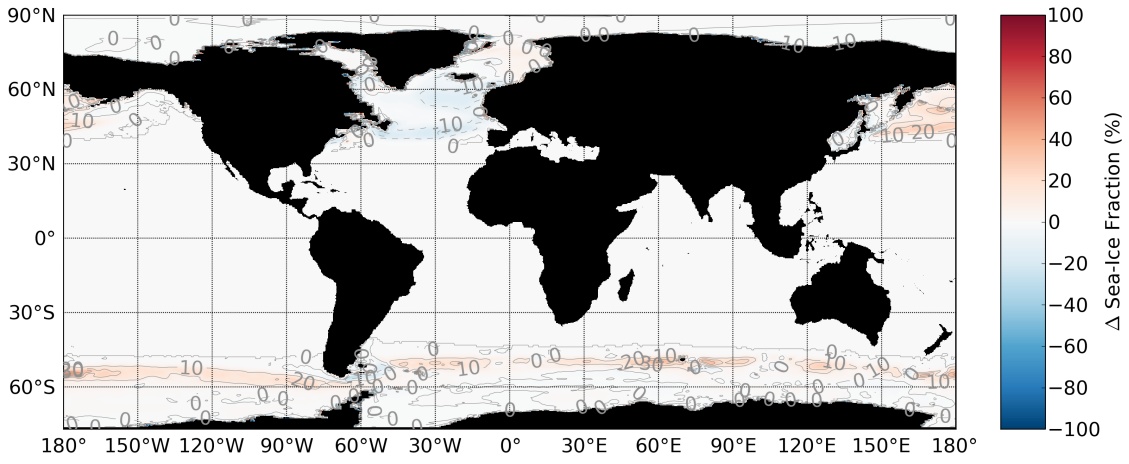


Figure S1: Annual mean difference in the sea-ice fraction between the coarse resolution and the eddy-permitting simulation. Units in %. The main difference occurs in the regions of eddies activity (similar to the Figure 1b in the manuscript)

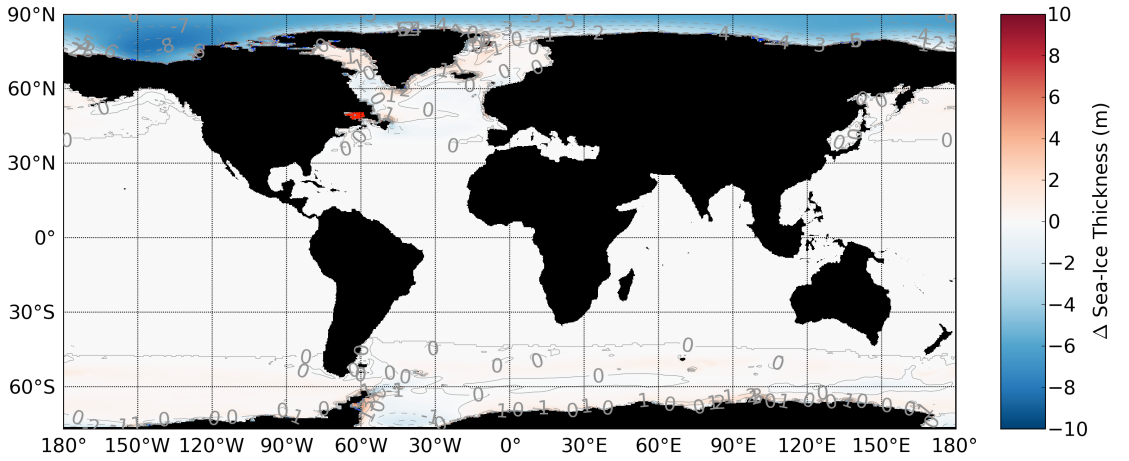


Figure S2: Annual mean difference in the sea-ice thickness between the coarse resolution and the eddy-permitting simulation. Units in m. The main difference is located in the Arctic basin. The sea-ice is about 8 meters thicker in the eddy-permitting simulation than in the coarse resolution

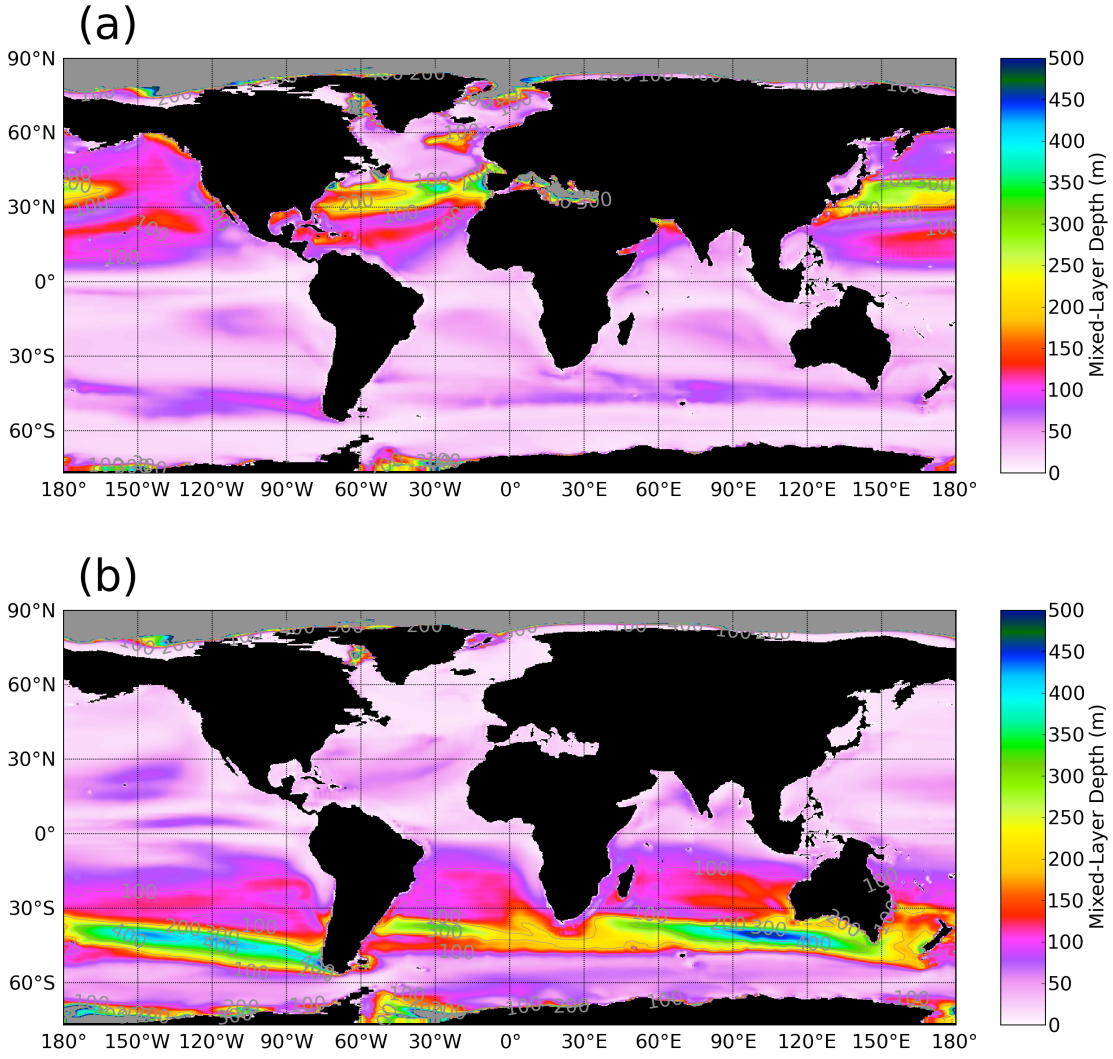


Figure S3: (a) Boreal winter (JFM) and (b) boreal summer (JAS) mixed layer depth (m) computed in the coarse resolution simulation. deep mixed layer are relatively similar to those for the eddy-permitting simulation except in the Arctic region. In the Arctic, the mixed layer depth (in grey) are greater than 500m due to the homogeneous temperature and salinity

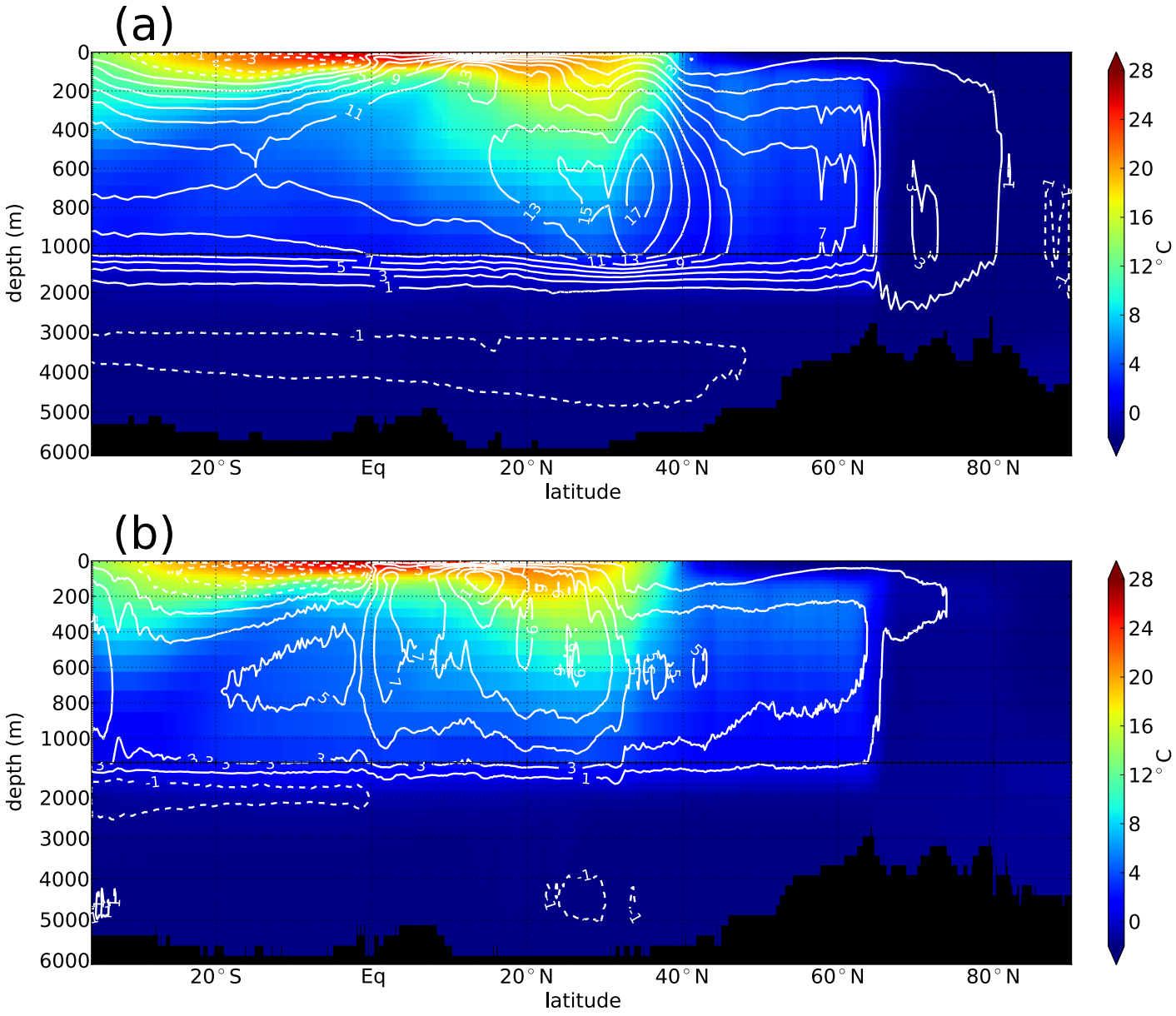


Figure S4: Atlantic Meridional Overturning Circulation (AMOC) computed for (a) the coarse resolution ORCA1 simulation and (b) the eddy-permitting ORCA025 simulation. Unit in Sv=$10^6 m^3.s^{-1}$. The time and zonally averaged temperature (°C) are represented in the background. The structure of the zonally averaged temperature in the Atlantic basin are relatively similar between the two experiments, contrary to the salinity structure (cf. Fig.7)

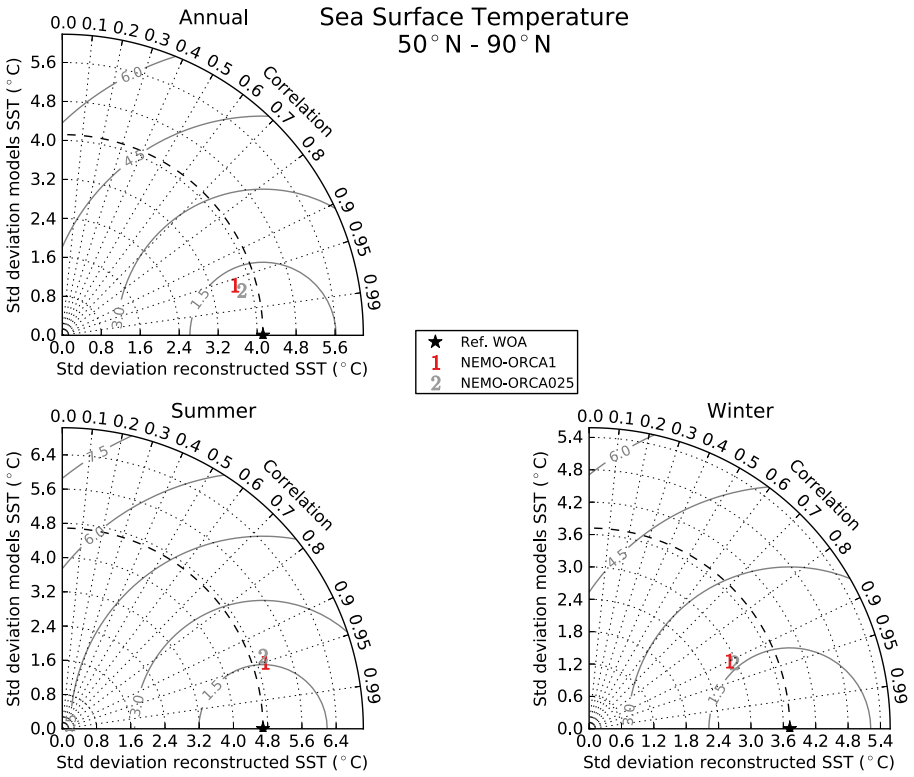


Figure S5: Taylor diagrams summarizing the correlation coefficient (along the arc), the standard deviations (on the axis) and RMSE (gray solid arcs of circles) for the Present-Day annual, boreal winter (JFM) and boreal summer (JAS) modeled and observed (World Ocean Atlas 1998) **global** sea surface temperatures between 50 and 90°N. The NEMO-ORCA1 is symbolized with the number 1, NEMO-ORCA025 with the symbol 2

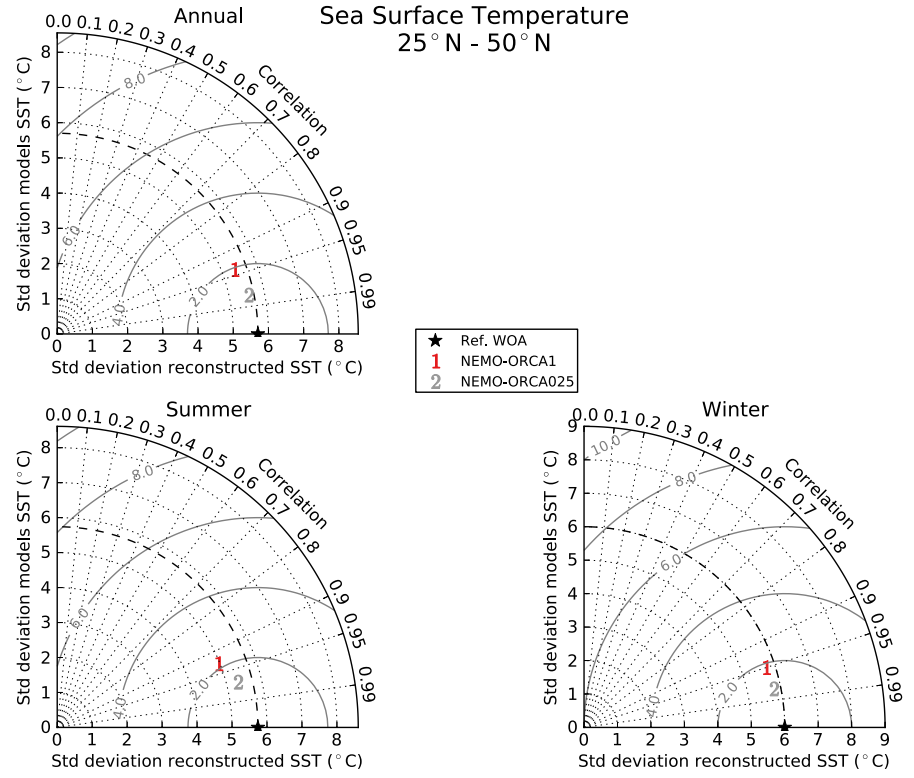


Figure S6: Taylor diagrams summarizing the correlation coefficient (along the arc), the standard deviations (on the axis) and RMSE (gray solid arcs of circles) for the Present-Day annual, boreal winter (JFM) and boreal summer (JAS) modeled and observed (World Ocean Atlas 1998) **global** sea surface temperatures between 25 and 50°N. The NEMO-ORCA1 is symbolized with the number 1, NEMO-ORCA025 with the symbol 2

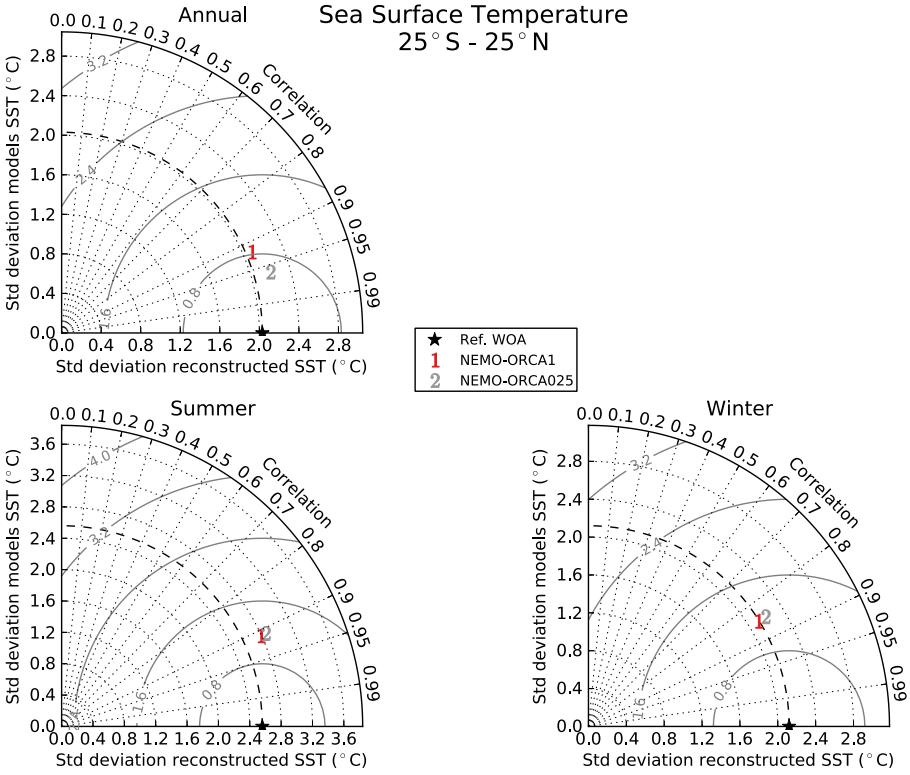


Figure S7: Taylor diagrams summarizing the correlation coefficient (along the arc), the standard deviations (on the axis) and RMSE (gray solid arcs of circles) for the Present-Day annual, boreal winter (JFM) and boreal summer (JAS) modeled and observed (World Ocean Atlas 1998) **global** sea surface temperatures between 25°S and 25°N. The NEMO-ORCA1 is symbolized with the number 1, NEMO-ORCA025 with the symbol 2

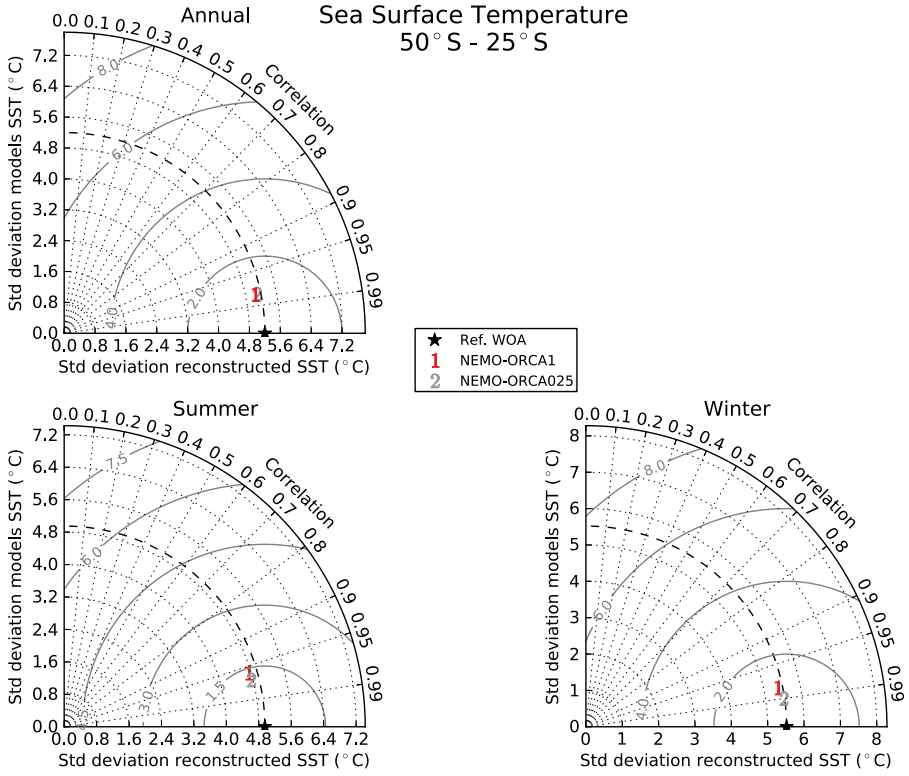


Figure S8: Taylor diagrams summarizing the correlation coefficient (along the arc), the standard deviations (on the axis) and RMSE (gray solid arcs of circles) for the Present-Day annual, boreal winter (JFM) and boreal summer (JAS) modeled and observed (World Ocean Atlas 1998) **global** sea surface temperatures between 50 and 25°S. The NEMO-ORCA1 is symbolized with the number 1, NEMO-ORCA025 with the symbol 2

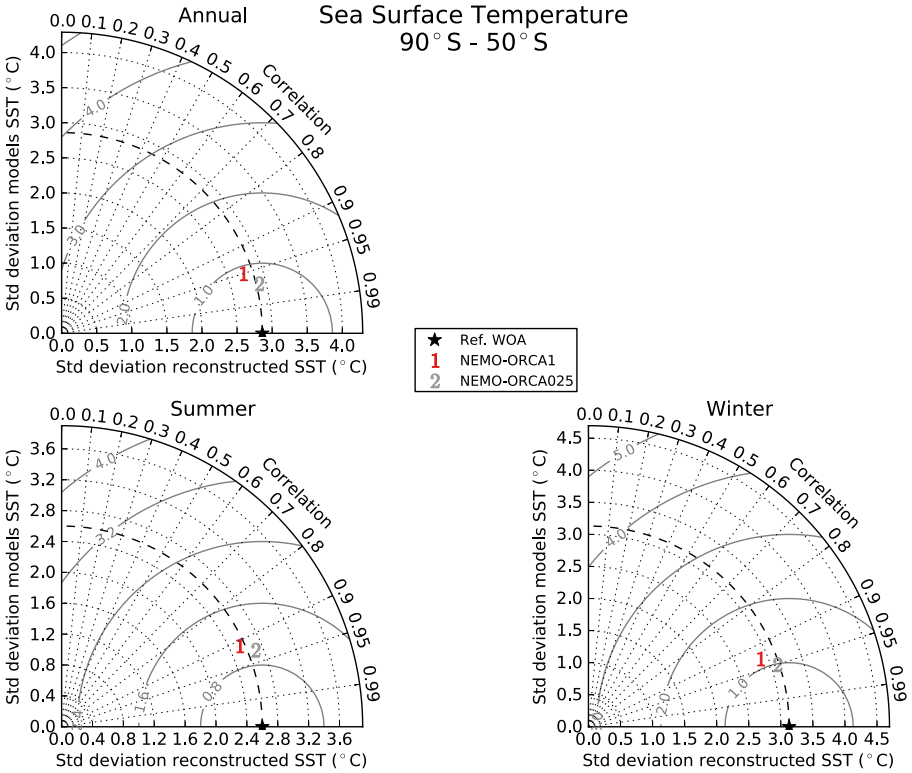


Figure S9: Taylor diagrams summarizing the correlation coefficient (along the arc), the standard deviations (on the axis) and RMSE (gray solid arcs of circles) for the Present-Day annual, boreal winter (JFM) and boreal summer (JAS) modeled and observed (World Ocean Atlas 1998) **global** sea surface temperatures between 90 and 50°S. The NEMO-ORCA1 is symbolized with the number 1, NEMO-ORCA025 with the symbol 2

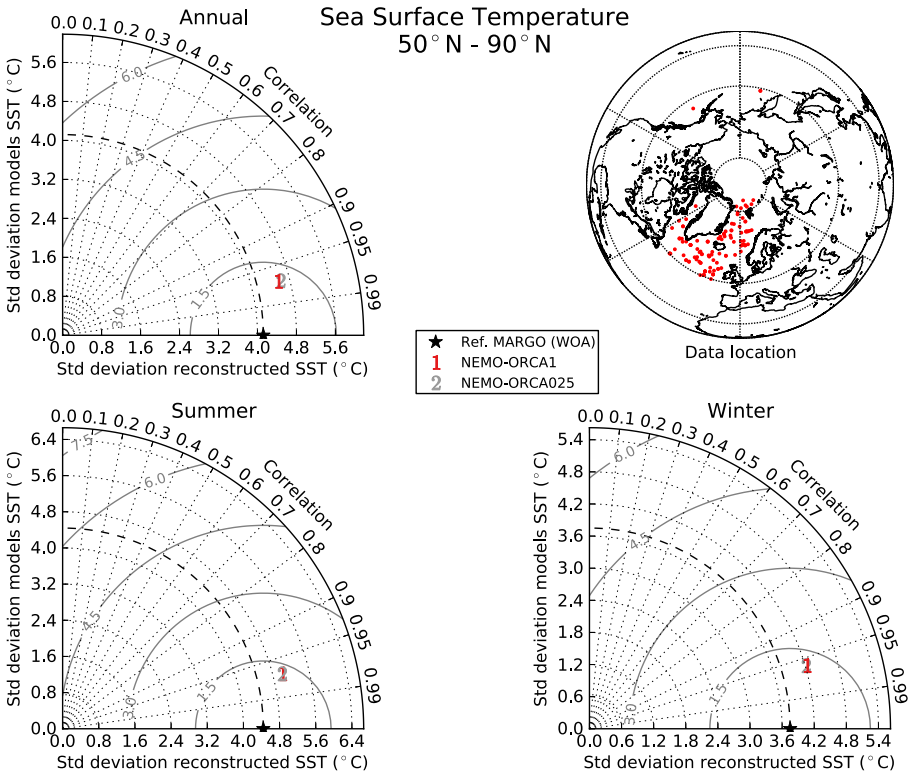


Figure S10: Taylor diagrams summarizing the correlation coefficient (along the arc), the standard deviations (on the axis) and RMSE (gray solid arcs of circles) for the Present-Day annual, boreal winter (JFM) and boreal summer (JAS) modeled and observed (World Ocean Atlas 1998) sea surface temperatures **at the MARGO core location** between 50 and 90°N. The proxy-data locations are shown in the upper right-hand diagram. The NEMO-ORCA1 is symbolized with the number 1, NEMO-ORCA025 with the symbol 2

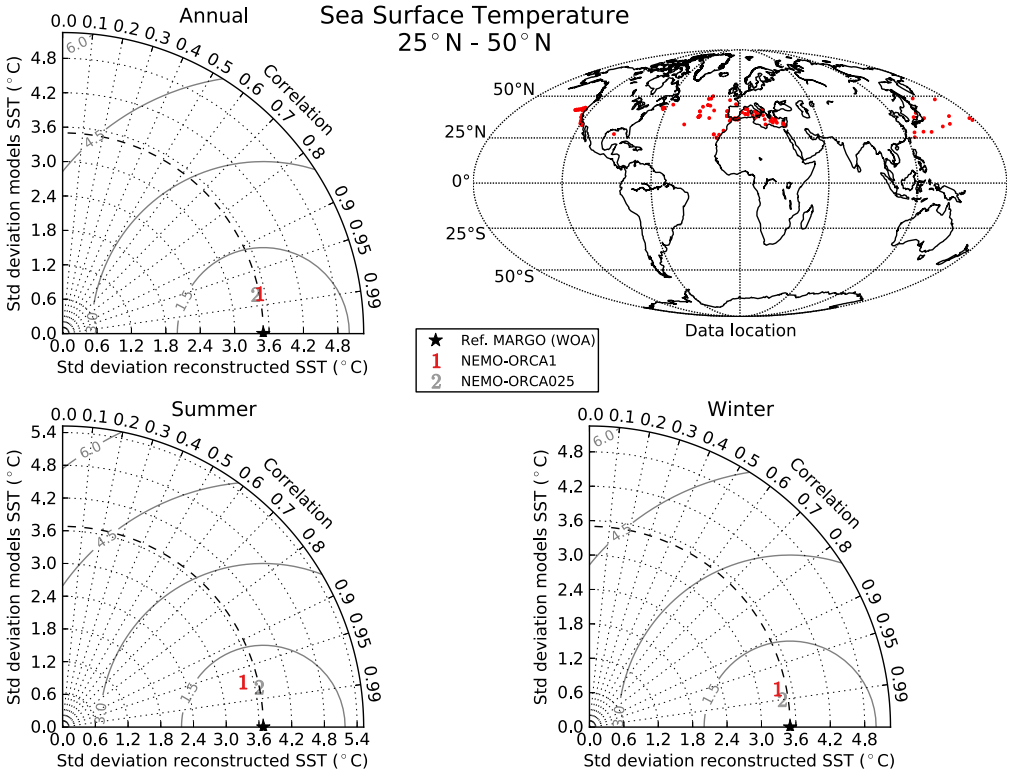


Figure S11: Taylor diagrams summarizing the correlation coefficient (along the arc), the standard deviations (on the axis) and RMSE (gray solid arcs of circles) for the Present-Day annual, boreal winter (JFM) and boreal summer (JAS) modeled and observed (World Ocean Atlas 1998) sea surface temperatures **at the MARGO core location** between 25 and 50°N. The proxy-data locations are shown in the upper right-hand diagram. The NEMO-ORCA1 is symbolized with the number 1, NEMO-ORCA025 with the symbol 2

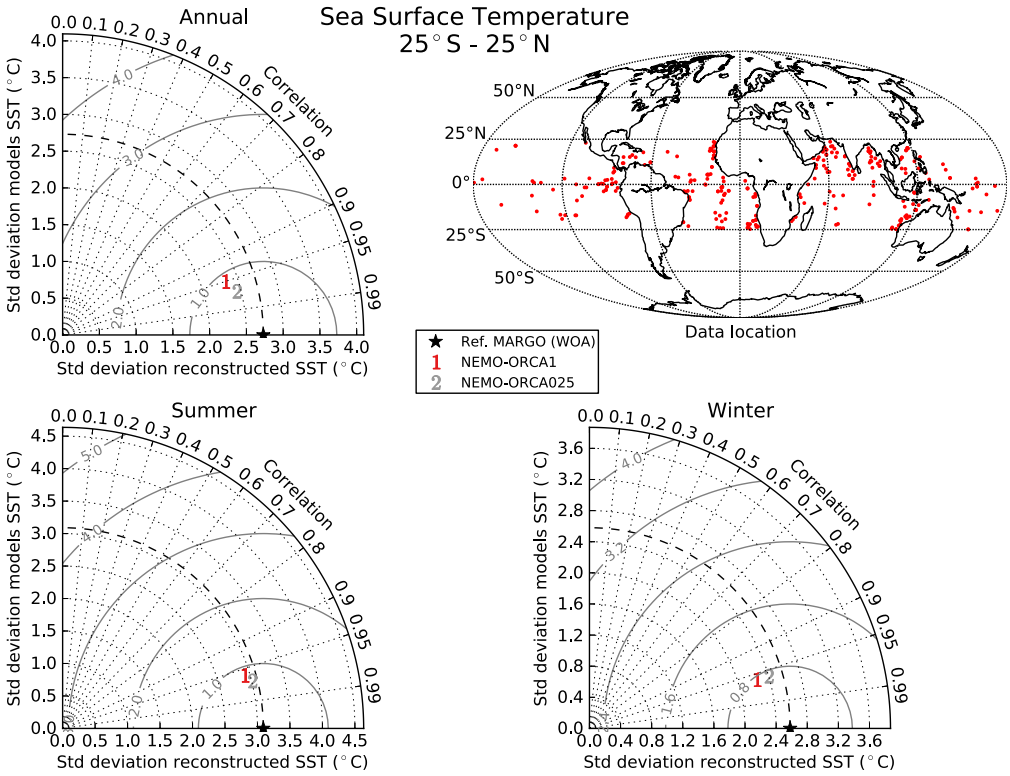


Figure S12: Taylor diagrams summarizing the correlation coefficient (along the arc), the standard deviations (on the axis) and RMSE (gray solid arcs of circles) for the Present-Day annual, boreal winter (JFM) and boreal summer (JAS) modeled and observed (World Ocean Atlas 1998) sea surface temperatures **at the MARGO core location** between 25°S and 25°N. The proxy-data locations are shown in the upper right-hand diagram. The NEMO-ORCA1 is symbolized with the number 1, NEMO-ORCA025 with the symbol 2

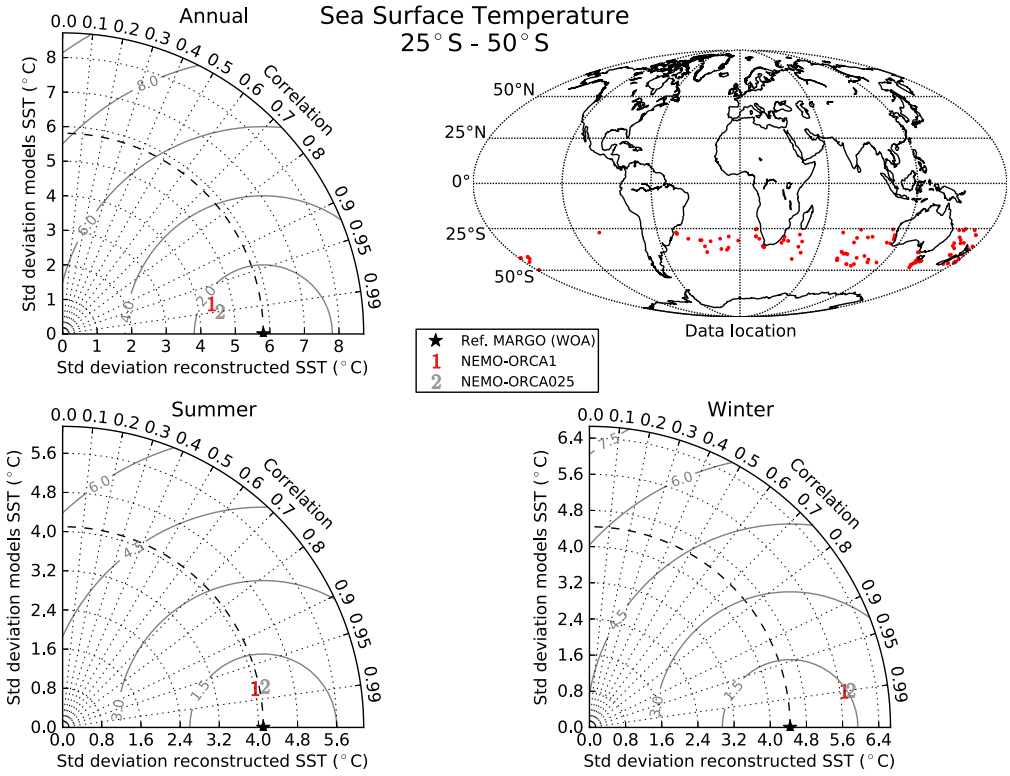


Figure S13: Taylor diagrams summarizing the correlation coefficient (along the arc), the standard deviations (on the axis) and RMSE (gray solid arcs of circles) for the Present-Day annual, boreal winter (JFM) and boreal summer (JAS) modeled and observed (World Ocean Atlas 1998) sea surface temperatures **at the MARGO core location** between 50 and 25°S. The NEMO-ORCA1 is symbolized with the number 1, NEMO-ORCA025 with the symbol 2

Table S1: Regional statistical analysis (linear regression test) between the simulated and observed (WOA98) SSTs summarized by the p-value, the correlation coefficient, the slope and the intercept (in °C) of the regression line. N is the sample size of the regional MARGO core sample location for each period. In bold, the most significant values

| | | ANNUAL | | WINTER (JFM) | | SUMMER (JAS) | |
|---|---|---|---|---|---|---|---|
| | | ORCA1 | ORCA025 | ORCA1 | ORCA025 | ORCA1 | ORCA025 |
| Agulhas (30°E-50°E; 50°S-10°S) $N^{ANN}$=14, $N^{JFM}$=14, $N^{JAS}$=10 | p-value | <**0.001** | <**0.001** | <**0.001** | <**0.001** | <**0.001** | <**0.001** |
| | $R^2$ | 0.97 | **0.99** | 0.99 | **1.00** | 0.94 | **0.98** |
| | slope | 0.92 | **1.05** | 0.95 | **0.99** | 0.88 | **1.00** |
| | intercept (°C) | 2.4 | **-0.98** | 1.27 | **0.36** | 2.70 | **0.04** |
| Gulf Stream (70°W-20°W; 30°N-45°N) $N^{ANN}$=19, $N^{JFM}$=12, $N^{JAS}$=12 | p-value | <**0.001** | <**0.001** | <**0.001** | <**0.001** | <**0.001** | <**0.001** |
| | $R^2$ | 0.97 | **0.99** | **0.99** | **0.99** | **0.99** | **0.99** |
| | slope | 0.79 | **1.01** | 3.54 | **0.96** | **0.94** | 1.14 |
| | intercept (°C) | 3.88 | **-0.20** | 0.77 | **0.43** | **1.10** | -3.49 |
| Kuroshio (120°E-160°E; 20°N-35°N) $N^{ANN}$=6, $N^{JFM}$=6, $N^{JAS}$=6 | p-value | **0.001** | 0.006 | **0.003** | 0.02 | <**0.001** | <**0.001** |
| | $R^2$ | **0.93** | 0.88 | **0.91** | 0.77 | **0.98** | 0.86 |
| | slope | 1.30 | **1.04** | 1.46 | **1.07** | **1.09** | 0.88 |
| | intercept (°C) | -6.75 | **-0.76** | -8.75 | **-1.53** | **-2.64** | 3.36 |
| SO-Atlantic (60°W-0°;45°S-60°S) $N^{JFM}$=30 | p-value | | | <**0.001** | <**0.001** | | |
| | $R^2$ | | | **0.97** | 0.94 | | |
| | slope | | | 0.87 | **0.94** | | |
| | intercept (°C) | | | 1.07 | **0.68** | | |
| SO-Africa (0°-50°;45°S-60°S) $N^{JFM}$=26 | p-value | | | <**0.001** | <**0.001** | | |
| | $R^2$ | | | **0.97** | 0.96 | | |
| | slope | | | **1.04** | 1.05 | | |
| | intercept (°C) | | | 0.31 | **-0.21** | | |
| SO-Indian (50°E-100°E;45°S-60°S) $N^{ANN}$=4, $N^{JFM}$=15, $N^{JAS}$=4 | p-value | **0.01** | 0.08 | <**0.001** | <**0.001** | **0.01** | 0.1 |
| | $R^2$ | **0.98** | 0.85 | **0.99** | 0.98 | **0.98** | 0.76 |
| | slope | 0.82 | **0.98** | 0.89 | **0.94** | 0.80 | **0.91** |
| | intercept (°C) | 1.10 | **-0.71** | 0.68 | **0.09** | 0.71 | **-0.49** |
| SO-Pacific (180°W-0°;45°S-60°S) $N^{JFM}$=40 | p-value | | | <**0.001** | <**0.001** | | |
| | $R^2$ | | | **0.96** | 0.95 | | |
| | slope | | | 0.84 | **0.93** | | |
| | intercept (°C) | | | 1.12 | **0.77** | | |

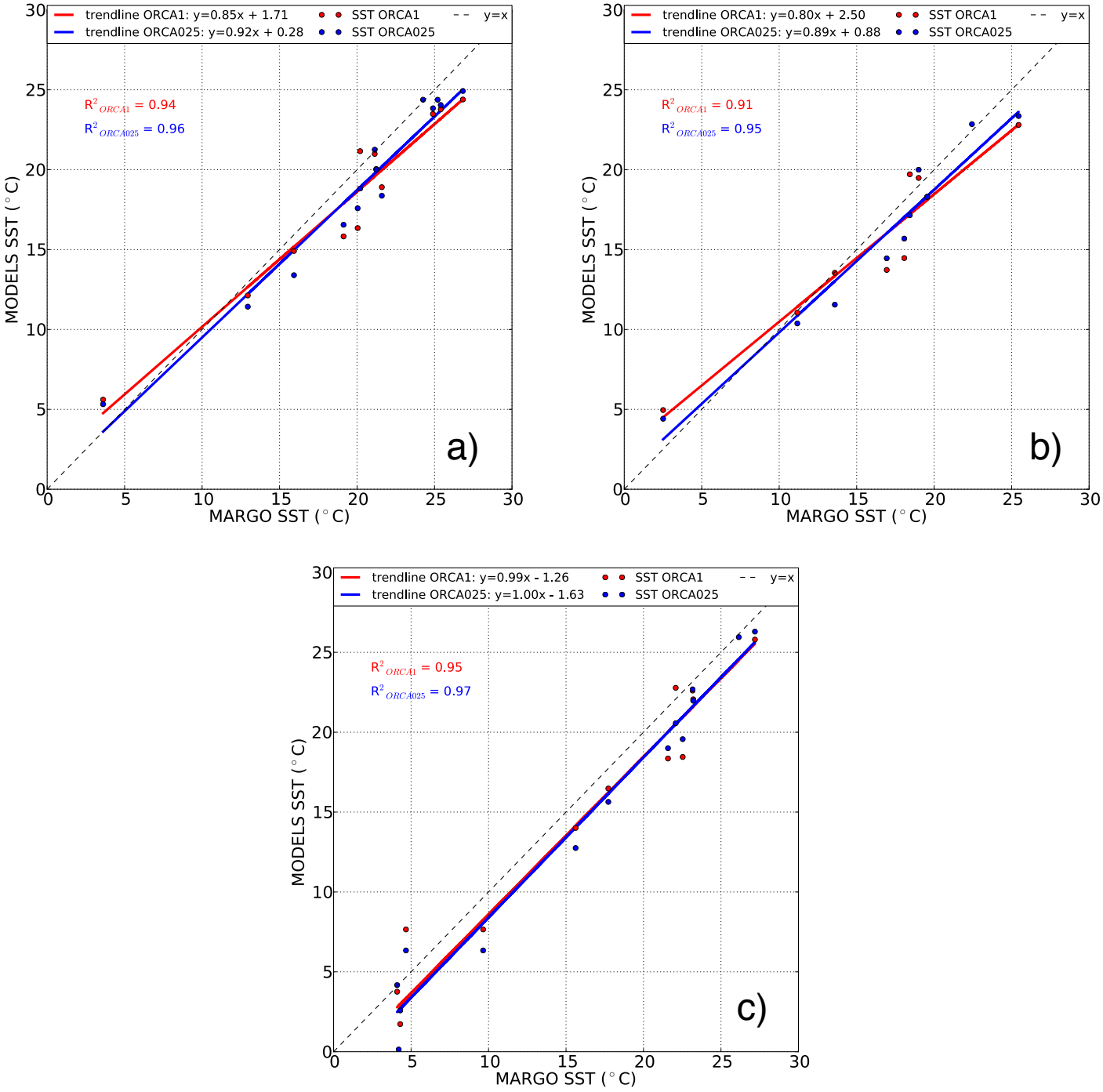


Figure S14: Scatter plots of the simulated ORCA1 and ORCA025 SSTs versus reconstructed SST in the **Agulhas region (30°E-50°E, 50°S-10°S)** for a) the ANN, b) the JAS and c) the JFM periods. On each diagram, the equation of the regression line and corresponding correlation coefficient R are given. The dashed line represents the y=x equation, *i.e.* the best correlation line.

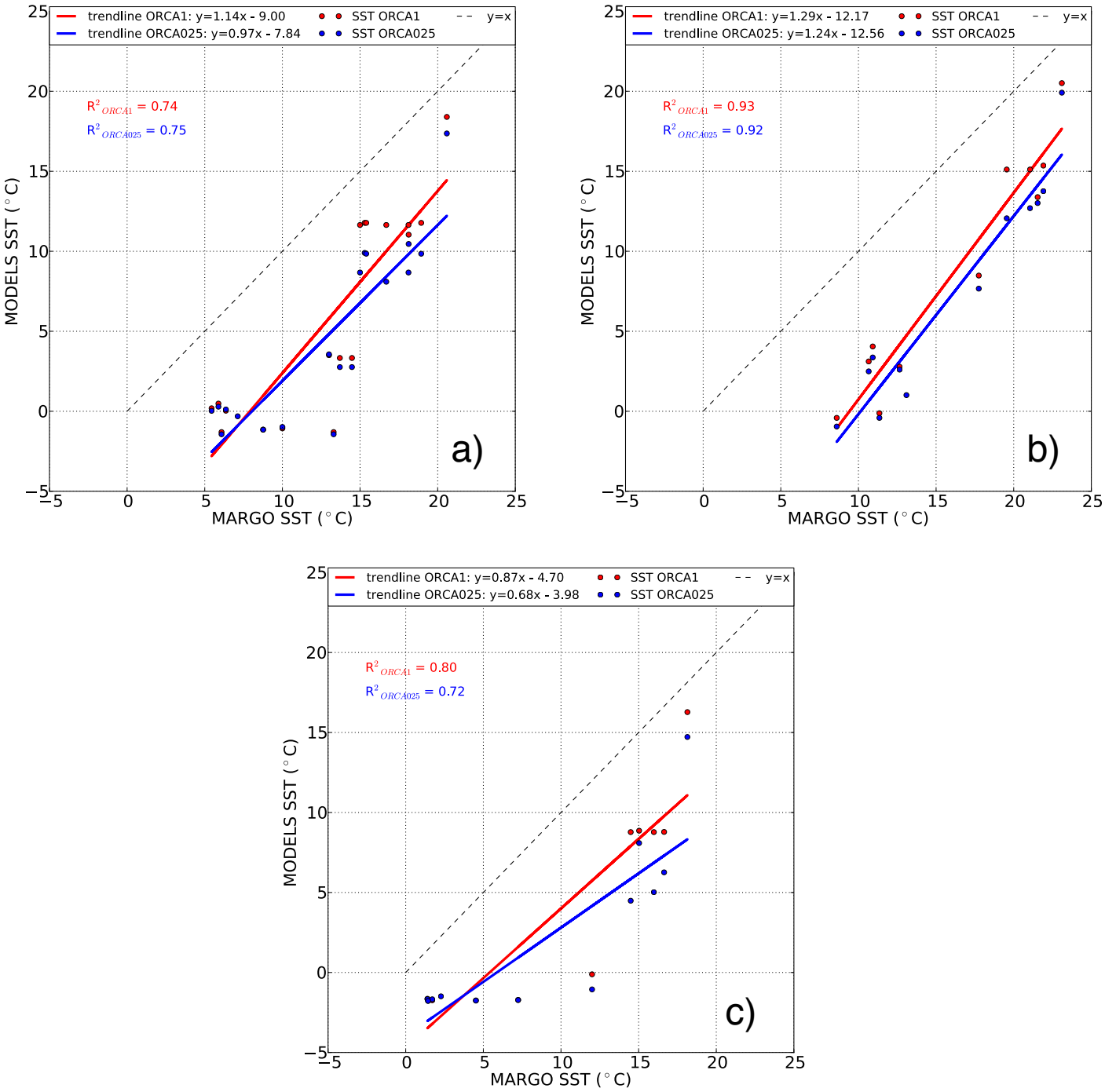


Figure S15: Scatter plots of the simulated ORCA1 and ORCA025 SSTs versus reconstructed SST in the **Gulf Stream region (70°W-20W, 30°N-45°N)** for a) the ANN, b) the JAS and c) the JFM periods. On each diagram, the equation of the regression line and corresponding correlation coefficient R are given. The dashed line represents the y=x equation, *i.e.* the best correlation line.

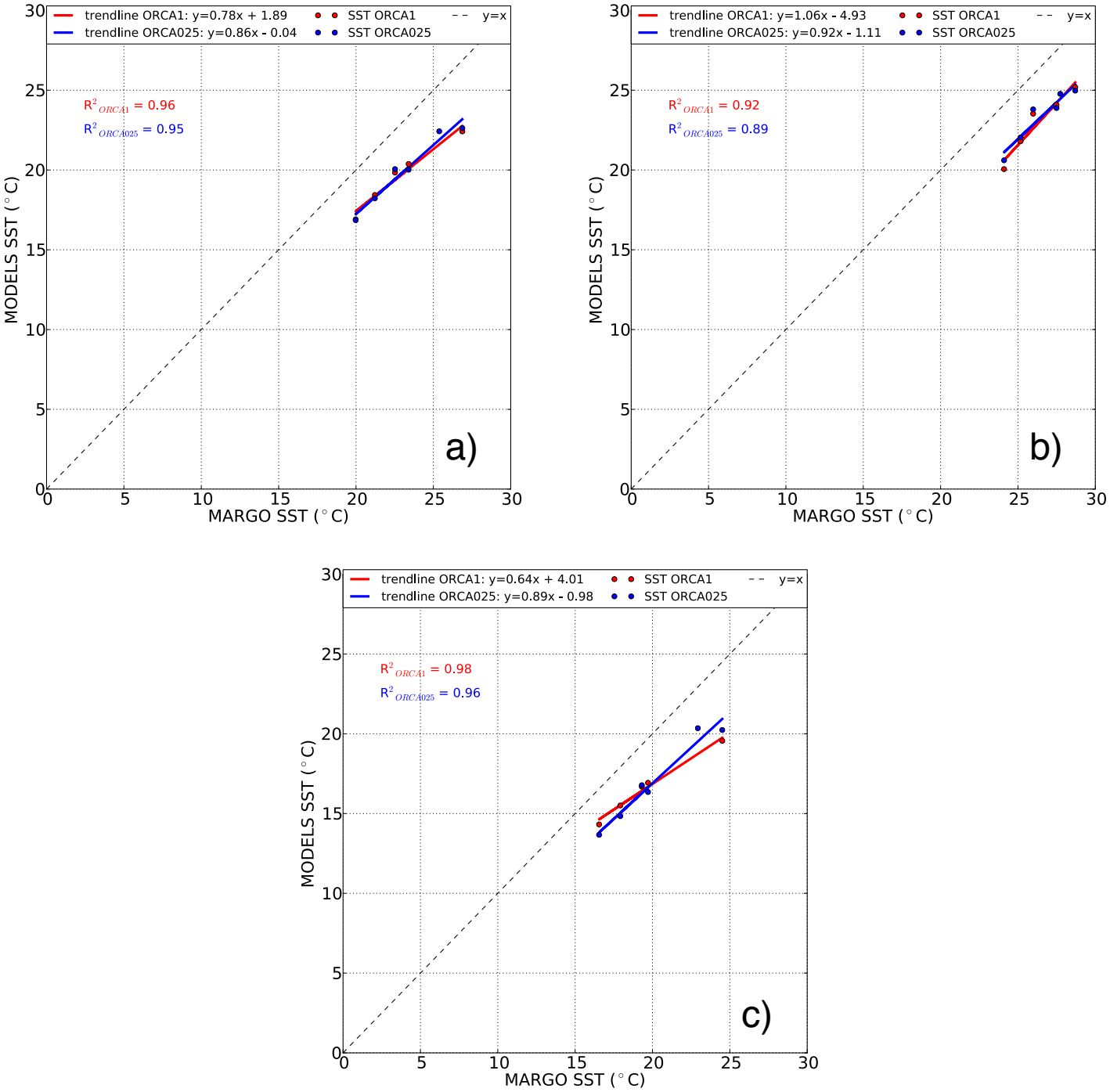


Figure S16: Scatter plots of the simulated ORCA1 and ORCA025 SSTs versus reconstructed SST in the **Kuroshio region (120°E-160W, 20°N-35°N)** for a) the ANN, b) the JAS and c) the JFM periods. On each diagram, the equation of the regression line and corresponding correlation coefficient R are given. The dashed line represents the y=x equation, *i.e.* the best correlation line.